AgRISTARS

SR-J0-04001
JSC-16829

A Joint Program for Agriculture and Resources Inventory Surveys Through Aerospace Remote Sensing

Supporting Research

October 1980

A SEMI-AUTOMATIC TECHNIQUE FOR MULTITEMPORAL CLASSIFICATION OF A GIVEN CROP OF A LANDSAT SCENE

G. D. Badhwar
National Aeronautics and Space Administration
Houston, Texas 77058

W. W. Austin and J. G. Carnes
Lockheed Engineering and Management Services Company, Inc.
1830 NASA Road 1, Houston, Texas 77058

Lyndon B. Johnson Space Center
Houston, Texas 77058

1. Report No.	2. Government Accession No.	3. Recipient's Catalog No.
JSC-16829; SR-J0-04001		

4. Title and Subtitle	5. Report Date
A Semi-Automatic Technique for Multitemporal Classification of a Given Crop	October 1980
	6. Performing Organization Code SF311

7. Author(s)	8. Performing Organization Report No.
G. D. Badhwar, W. W. Austin and J. B. Carnes	
	10. Work Unit No.

9. Performing Organization Name and Address		11. Contract or Grant No.
Earth Observations Division Supporting Research Branch NASA Johnson Space Center Houston, Texas 77058	Lockheed Engineering and Management Services Co., Inc. 1830 NASA Road 1 Houston, Texas 77058	
		13. Type of Report and Period Covered
12. Sponsoring Agency Name and Address National Aeronautics and Space Administration Lyndon B. Johnson Space Center Houston, Texas 77058		14. Sponsoring Agency Code

15. Supplementary Notes

16. Abstract

A classification scheme based on temporal characteristics of a given crop is described. The technique in its present form requires one training field of the crop under consideration. This training field is used to analytically determine the time behavior of the crop (in the LACIE segment). A comparison of this crop temporal profile, generated in each of the Landsat channels, with that of every pixel in the segment is made to decide the category (crop/noncrop) of the pixel. Classification results have been compared with ground truth for thirty four sites in the U.S. Corn Belt. This technique has the potential for a more automated method of generating a near-harvest crop inventory from the satellite data than the inventory method in current use.

17. Key Words (Suggested by Author(s))	18. Distribution Statement

19. Security Classif. (of this report)	20. Security Classif. (of this page)	21. No. of Pages	22. Price*
Unclassified	Unclassified		

*For sale by the National Technical Information Service, Springfield, Virginia 22161

A SEMI-AUTOMATIC TECHNIQUE FOR MULTITEMPORAL CLASSIFICATION OF A GIVEN CROP OF A LANDSAT SCENE

G. D. Badhwar
National Aeronautics and Space Administration
Lyndon B. Johnson Space Center
Houston, Texas 77058

and

W. W. Austin and J. G. Carnes
Lockheed Engineering and Management Services Company Inc.
1830 NASA Road 1
Houston, Texas 77058

I. Introduction.

Current approaches to the inventories of global crops from satellites depend almost totally on the judgment and skills of an image analyst. The input, in the form of analyst labelled pixels or groups of pixels, is used to train a computer classification program. These approaches are very time consuming. If routine global inventories from satellites are to become a reality, a considerable reduction, if not the elimination of human interpretation, in crop identification will be necessary.

The current approaches to the inventories of global crops from remotely sensed data relies on simple Gaussian statistical structure (Fu, Landgrebe, and Philips [1]). This implicitly assumes that the phenological growth stage for each vegetation subclass is the same for all observations made at a given time. However, even in a geomorphologically homogenous area, this assumption is known to be invalid and has been shown to lead to probability distributions that are not unimodal (Chikkara and Register [2]). It is also known that variation of phenological growth stages increases the variance of usual probability distribution by many times (Haralick et al [3], Badhwar [4]). Haralick et al, have developed a method of spectral-temporal classification that involves the creation of crop signatures which characterize multispectral observations as functions of phenological growth states. In this approach, for each possible crop category a correspondence of time to growth state is established that minimizes the smallest difference between the given multitemporal multispectral vector and the category mean vector indexed by growth state; the latter must be established in some independent manner, for example, crop calendar practices.

In this paper a new approach, based on an invariant-class of models, is proposed. This approach explicitly takes into account differences in the planting time which are one of the major causes of large variances and non unimodal

distributions. In this approach the analyst is used to define, using the Landsat imagery, a field of the crop of interest. The computer classification program is then "trained" on this field only and every pixel is classified as crop or non crop. This technique has been applied to 34 segments in the U.S. Cornbelt area to separate corn from other crops.

II. Temporal Model of Spectral Response

This approach to classification is based on the hypothesis that a given crop, after emergence, has a unique spectral shape in time (a profile). A crop exhibits emergence at different times over a site.. The result is displacement of the crop development profile, but not a change in its basic shape. This classification method incorporates the effects of planting time distribution and bases the classification on the profile of the crop. It is fully realized that many other agronomic variables, besides the planting time, can and will effect the shape of this profile. However, the effects of these variables are significantly reduced by local training; this is discussed in the next section.

The spectral reflectance in the 0.7-1.1 μm of a healthy plant of an annual crop is known to rise, peak, and fall as a function of time. In an earlier paper, Badhwar [4], suggested that this behaviour can be described by an incomplete gamma functional for the annual crops of spring wheat and spring barley. Independently, Crist and Malila [5] applied this functional form to the time behaviour of the Kauth-Thomas Greenness, (a linear combination of spectral reflectance). Recently, Rice et al [6] have applied this form to soybeans and Badhwar and Henderson [7] to the corn and soybean crops. The particular functional form for such a model is

$$\rho(t) = At^{\alpha} \text{ Exp } (-\beta t^2) \qquad (1)$$

where $\rho(t)$ is spectral response in a particular wavelength interval, α and β are crop and condition specific constants, and A is a normalization constant. The spectral response on emergence day $t = t_o$ should be equal to the spectral response of bare soil, $\rho_s(t_o)$, Thus equation (1) can be rewritten as

$$\rho(t) = \rho_s(t_o)\ (t/t_o)^{\alpha} \text{ Exp } \left\{\beta(t_o^2 - t^2)\right\} \qquad (2)$$

This analytic description of the spectral response henceforth will be called a spectral profile. It was shown by Badhwar [4] that within a LACIE segment if the crop emerges late (or early) relative to a reference field, the profile is displaced but has the same basic shape as that of the reference field. This model of the temporal characteristics of the reflectance is used as a basis for the classification of the crop under consideration. The model has four free parameters ρ_s, α, β and t_o that are determined from the application area that is to be classified.

III. Approach

A training area of the crop that is to be classified is selected from the LACIE segments by an analyst. This area is the interior of a field of the crop of interest. This step is analogous to what is commonly referred to as extrapolation mode (Steiner and Salerno, [8]). The obvious advantages of this mode are (i) less exact calibration capability of the system sensors is required, and (ii) less exact knowledge of other experimental variables is necessary since only variations of these factors within the segment need be accounted for. For example, atmospheric correction do not have to be rigorously determined. [This, of course, does not imply that the reduction of spatially varying atmospheric effects would not improve the data quality].

The major disadvantage of this approach, as of any other technique in use at present in remote sensing, is prior knowledge of the scene to be classified.

The training area is screened for obvious outlier pixels. For each Landsat band, the mean, μ, and the standard deviation, σ, of the spectral values over each acquisition day of interest are computed. The criterion for rejecting a pixel is that channel value, $\eta(t)$, on the acquisition day, t, does not satisfy the inequality $[\mu(t) - 3\sigma(t)], < \eta(t) < [\mu(t) + 3\sigma(t)]$. This is a fairly liberal criteria, especially if one considers the fact that outlier pixels would distort the "true" $\mu(t)$ values. If the pixel is an outlier in any Landsat band on any of the acquisition days, it is removed from further consideration. After rejecting these outlier pixels, the mean and standard deviation of the remaining pixels are recomputed.

Having determined the means and standard deviations in individual Landsat bands over the acquisitions, the temporal model of equation (2) is fitted iteratively using the algorithm of Marquardt [9] to determine the four free parameters.

The fitted curves are the nominal temporal profiles of the crop and are assumed to apply to every pixel of the same crop in the scene except that different pixels may have different values of the emergence date t_o. However, before this nominal profile can be used for classification of individual pixels, the "measurement" error (sensor + scene noise) and the error associated with determining the nominal profile must be included.

IV. Classification.

Consider a modified distance function, $\psi_j^2(\tau)$, defined by

$$\psi_j^2(\tau) = \frac{1}{N} \sum_{i=1}^{N} \left\{ \frac{\rho_{cal}^j(t_i) - \rho_{ob}^j(t_i)}{\sigma^j(t_i)} \right\}^2 \qquad (3)$$

where $\rho^j_{cal}(t_i)$ is the calculated channel value in Landsat band j, (using the fitted constant ρ_s, t_o, α and β obtained from training field) $\rho^j_{ob}(t_i)$ is observed channel value on acquisition day t_i, $\sigma_j(t_i)$ is the "measurement noise" in band j on day t_i. τ is the emergence date of pixel which is determined by minimizing $\Psi^2_j(\tau)$. This corresponds to the physical condition that the emergence date of the pixel can be different from that of the "nominal" emergence date. N is the number of acquisitions.

The classification scheme is based on this distance function. It is basically a measure of how far (in units of standard deviation) the temporal profile of an individual pixel lies away from the "nominal" profile of crop as determined from the training area. This distance function is dimensionless and if $\rho^j_{ob}(t_i)$ is normally distributed with mean $\rho^j_{cal}(t_i, \tau)$ and standard deviation $\sigma_j(t_i)$, then $[\Psi^2_j(\tau)]$ and standard deviation $\sigma_j(t_i)$, then $[\Psi^2_j(\tau)]_{min}$ has a chi-square distribution with (N-1) degress of freedom.

In order to use this distance measure for classifying individual pixels one needs to (i) determine what $\sigma_j(t_i)$ to assign to an individual pixel and, (ii), determine the threshold boundary, Ψ^2_{th}, above which a pixel is unlikely to be that of the crop under consideration.

a. Noise. Figure 1 shows a plot of sensor noise as a function of input channel value [10]. In Landsat band 1, 2, and 3, the noise is proportional to (signal level)$^{1/2}$ as expected and that in CH 4 is a constant. This provides then the absolute minimum of the noise $\sigma_j(t_i)$ on any given date. In addition to this, there is a scene noise due to the variance in the optical depth caused by changes in the particulate size distribution (λ = 0.35 -.7 μm) and in the infrared (.9 - 2.4 μm)due to the water vapor distribution. Duggin [11] from extensive measurements made over desert areas in the 0.5 - 0.6 μm band shows that σ (scene)$\approx$(.07 - .18) x signal level. Pitts [12] has indicated that σ (scene) $\approx$0.07 x signal level due to water vapor distribution. Additional sources of

scene "noise" arise due to the plowing pattern used, surface-drainage variation, the solar azimuthal and elevation angles and the direction of the furrows with respect to the line of sight of the sensor [13]. If one simply includes the lowest value of above reported noise, one finds then that the $\sigma_j^{min}(t_i) \geq \left[\sigma^2_{sensor} + \sigma^2_{scene}\right]^{1/2} \approx 1.5\ \sigma_j(sensor)$. It is, therefore, assumed that $\sigma_j(t_i) = Max\ \left[\sigma_j^{min}(sensor), \sigma_j(training\ field)\right]$. It should, however, be noted that some uncertainty remains in the knowledge of $\sigma_j(t_i)$.

b. Thresholding. A decision rule must be specified to determine when the multitemporal profile of the pixel under consideration is dissimilar from the temporal profile of the crop under consideration. For classification using $[\psi^2_j(\tau)_{min}$ this rule is specified by the numerical value, ψ^2_{th}. If the minimized value of $[\psi^2_j(\tau)]_{min}$ is less than ψ^2_{th} the pixel is classified as the crop of the training field and not otherwise.

The value of this threshold is determined directly from the training field itself. Using equation (3) and constants $\rho_s(t_o)$, α and β and the noise determined in the section above, the distribution of ψ^2_{min} over all of the pixels in training field is determined. Figure 2 shows one such distribution. (The distribution in ten other segments is rather similar). However, this distribution is not the standard chi-square distribution with (N-1) degrees of freedom. Let ξ_{max} be the maximum value of ψ^2_{min} in the training field data. Thus, the threshold has to be at least as large as ξ_{max}. But it is clear, that if the numbers of pixels in training field is rather small, it is unlikely to reflect the tail end of the distribution. Moreover, variations cuased by fertilization history, genetic variety, humidity and water

stress are all likely to cause a variation that is likely to push the value of threshold to be higher than ξ_{max}. One of the causes why $\psi^2_{min}(\tau)$ is not a chi-square distribution is due to the fact that one does not know the true value of $\sigma_j(t_i)$. From equation (3), it is seen that this uncertainty simply leads to a multiplicative factor, c, on $\psi^2_{min}(\tau)$. The hypothesis that distribution of observed $\psi^2_{min}(\tau)$ for training is indeed a chi-square distribution, except for the scale factor, can be studied by applying the Kolmogrov-Smirnov [14] test to the data. The scale factor can be estimated using a maximum likelihood analysis and is found to be simply given by

$$c \equiv (\text{Mean of } \psi^2_{min}(\tau) \text{ values of the field})/\text{Degrees of freedom.}$$

A check of the hypothesis that the observed values of ψ^2_{min} in individual Landsat channel is a "scaled" chi-square distribution was performed on 20 fields of corn and wheat scattered over segments spanning a large geographic area and found to hold well. Using the chi-square table, the threshold is set at 0.025% rejection level. In addition, one requires that the value of τ determined for a pixel satisfy the inequality $[t_o-20] < \tau < [t_o+20]$. That is, the calculated emergence date of a pixel must be within $\pm$ 20 days of that of "nominal" crop as established by the training field.

Knowing the temporal profile of the crop under consideration, an estimate of the "measurement" noise of the signal for an individual pixel and distance threshold, the classification of a segment can be done.

In the next section, the method followed in the site and training field selection is discussed.

V. Analyst Input: Training Field Selection and Choice of Acquisitions.

The analyst provided the input for the classification procedure discussed above using the LACIE film products. These products display spectral values in 3 channel combinations; and provide a practical means of identifying spectral signatures and separating spatial features. Figure 3 is an example of LACIE film product depicting Landsat Channel 1, 2, and 4, color coded blue, green, and red. Using these products the analyst selects four (preferably five) acquisitions for use in the classification. The selection criteria for the acquisitions are; (1) reasonably haze-free and cloud-free, (2) with a $\pm$ 1 pixel MSE multitemporal registration error and (3) of acceptable data quality and (4) are sufficiently well distributed in time to characterize the growth cycle of the crop in the post emergence to pre-harvest growth stages.

Having selected the acquisitions, the analyst correlates agricultural information for the geographical area of the segment to crop signature on the imagery (for example, approximate planting time, growth cycle, and harvest time). Using the change in relative channel reflectance over the crop growth cycle over the acquisitions a training field is selected (Figure 3). The training field selection criteria are (1) interior field size of 20 to 40 pixels, (2) border and edge pixels excluded, (3) no roads, evident drainage patterns, or other unusual features on the field of (4) a usual spectral signature (for example, not an irrigated field in an area of dry land farming).

A single analyst, using the above criteria selected four corn fields per segment is about 30 minutes. A comparison of the fields selected with the ground truth showed perfect agreement. Thus, the training field can be selected efficiently and accurately.

In order to ascertain that the selected field describes the growth cycle of the crop and the acquisition set is useable, the individual channel values were plotted as a function of the day of the year, Figure 4. If the fit of the model form of equation (2) shown in Figure 4 by the solid curve was satisfactory, this data was used for training field.

VI. Results and Discussion

Figure 5 gives the county distribution of 34 segments in the U.S. Corn Belt that were classified using the profile similarity technique presented above. These sites had reasonable acquisition histories and had available the aircraft photography ground truth which made it possible to check on the accuracy of the classification. The ground truth aircraft photography was delineated, fields identified and digitized in subpixel unit, such that 6 ground truth pixels correspond to one Landsat pixels.

Before discussing the results from all of the segments, the classification results of LACIE segment 0882 are presented. In section V, the Landsat imagery (Figure 3) and the method of selecting a training field from this segment were presented. The results of a pixel-by-pixel classification using the selected field are shown in Figure 6. Here, the blank spaces are pixels that are rejected by this method as not being corn and the filled out areas are classified as corn. This classification map is clean, that is, field patterns are quite evident and well filled out, and the blank areas do not show a random scattering of pixels. A comparison of the classification map with the observed ground truth map shown in Figure 7 shows that these fields are corn fields indeed.

Table I summarizes the results of all 34 segments. Column I gives the LACIE segment number, the county and state in which this geographic site is located. Column II gives the acquisition days and the training field used in the classification. Column III gives the confusion matrix, that is, the percentage of corn classified as corn, the percentage of corn classified as non-corn, percentage of non-corn classified as corn and percentage of non-corn classified

as non-corn. The total of these percentages add to 100% and represents the total number of pixels in the segments. These confusion matrix are presented in rows 1, 2, and 3 for all pixels and decreasingly pure pixels. Row 2 results are based on only those pixels in which all six of the subpixels of the digitized ground truth belong to the same category. Row 3 results are based on only those pixels which are the centers of a area 4 subpixels wide by 5 subpixels high having the same ground truth category. These represent essentially pixels interior to field. It should however be noted the digitized ground truth is registered to one base date which may or may not be one of the acquisitions dates used in this classification. Thus, misregistration errors are minimized as one goes from Row 1 to Row 3 but are not necessarily eliminated. It should also be pointed out that the data was not screened for clouds or cloud shadows, etc. These pixels along with those corn fields harvested (say for sillage) or hail damaged before the final acquisition day may be classified as non-corn, thus lowering the over all accuracy slightly. By averaging over all segments, one finds that percentage of corn correctly classified (PCC) as corn increasing from 64.1% to 73.7% and the percentage of non-corn classified as non-corn increases from 85.0% to 90.3%. Figure (8a) shows a scatter plot of PCC of corn for category 3 (Pure pixels) versus PCC for all pixels and Figure 8b shows the same for non-corn. It is clearly seen that percentages increase in going from all pixels to pure pixels as expected for all segments.

Finally, the purpose of any classifier is to determine the true proportion of the crop in the segment. Figure (8c) shows a scatter plot of the classifier determined proportion of corn versus the ground truth (GT) proportion. The results indicate a mean difference of (GT proportion - classifier proportion) of -2.97 ± 7.22, that is result which is essentially unbiased. Within the accuracy of these results the classifier is not found to be sensitive to the choice of the training field.

Conclusion

It has been shown that profile similarity classifier has the potential of being an effective classification procedure. The method has very simple training requirements and is very time efficient. The method, because of the fact, that areas are correctly identified fields, has the potential of improvements since the cause of misidentification can be traced.

Acknowledgement

One of us (GDB) is deeply thankful to Dr. A. H. Feiveson who pointed out that the Kolmogrov-Smirnov test be applied to the data and provided a card deck of his program for the same. We are also thankful to Drs. A. H. Feiveson, D. E. Pitts, K. E. Henderson, and A. G. Houston for suggestions and improvements in the paper. Mr. Gary L. Gutchewski of NASA/JSC selected the training fields.

Figure Captions

Figure 1. A plot of the standard errors (counts) versus the signal level (counts) for the four Landsat bands.

Figure 2. A histogram of the modified distance function $[\psi^2(\tau)]_{min}$ for a particular training field.

Figure 3. Figures 3a to 3e are a time sequence of film product imagery created from the Landsat spectral values, MSS channels 1, 2, and 4. For this product, the channel values are represented by the colors blue, green, and red respectively. Hence the temporal sequence illustrates the change in relative reflectance of the channel values as the growth stage of vegetation progresses.

The grid on each figure provides a reference for field location in the 196 pixel (picture element) by 117 line image. The coordinates (line, pixels) of the training field defined for this segment, s.s. 882, are (77, 77), 76, 84), (81, 87), (82-80). On June 8, 1978 acquisition, this field exhibits a grey-green signature indicative of approximately equal channel reflectance: a "bare soil" signature. On acquisition day July 5, the red signature indicates low reflectance in channels 1 and 2 (the chlorophyll absorption bands) relative to the high reflectance in the infrared band channel 4: a 'vigorous growth' signature. Acquisitions on August 10 and August 19 indicate diminishing of this relative difference, hence senescence of the corn in the field. Acquisition day September 22 exhibits a grey-brown signature indicative of ripe corn.

Figure 4. A plot of the mean and one standard deviation of the spectral values as a function of the acquisition day. The solid curve through the data points is the nonlinear fit to the model of equation (4), the constants of the fit and their respective errors are given at the top of each plot.

Figure 5. Geographical distribution of segments analyzed.

Figure 6. A pixel-by-pixel classification map of segment 0882. Dark areas are non-corn and light area is corn crop.

Figure 7. A pixel-by-pixel ground truth map of segment 0882. Dark areas are non-corn and light area are corn.

Figure 8. (a) A scatter plot of the percentage of corn correctly classified for all pixel versus that for pure (Row 3) pixels.

(b) A scatter plot of the percentage of non-corn correctly classified for all pixels versus that for pure pixels.

(c) A plot of the difference of ground truth proportion and classification proportion against ground truth proportion.

Each point in these figures corresponds to one segment.

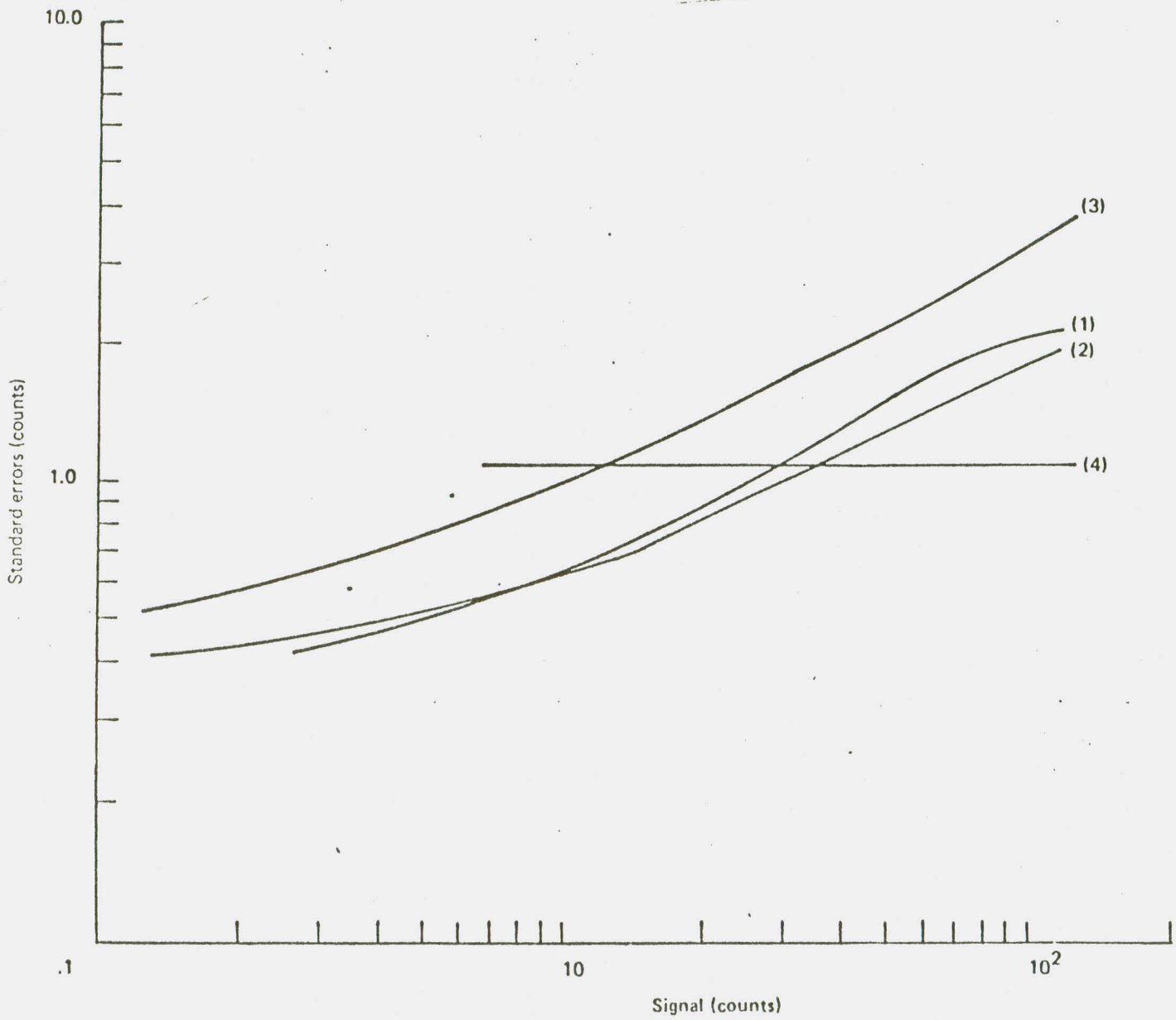

Figure 1

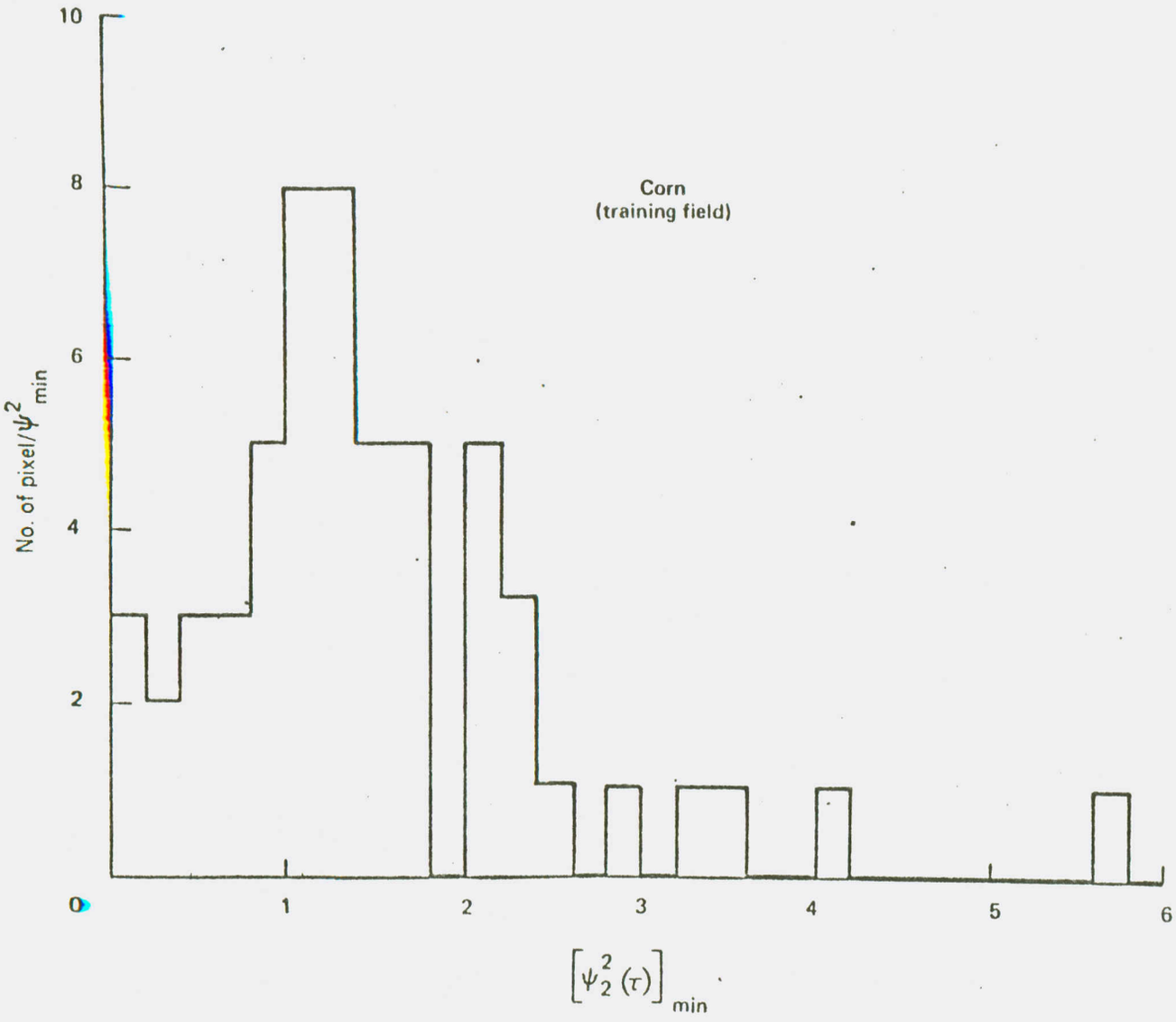
Corn
(training field)
No. of pixel/ψ^2_{min}
10
8
6
4
2
0
1
2
3
4
5
6
$\left[\psi_2^2(\tau)\right]_{min}$

Figure 2

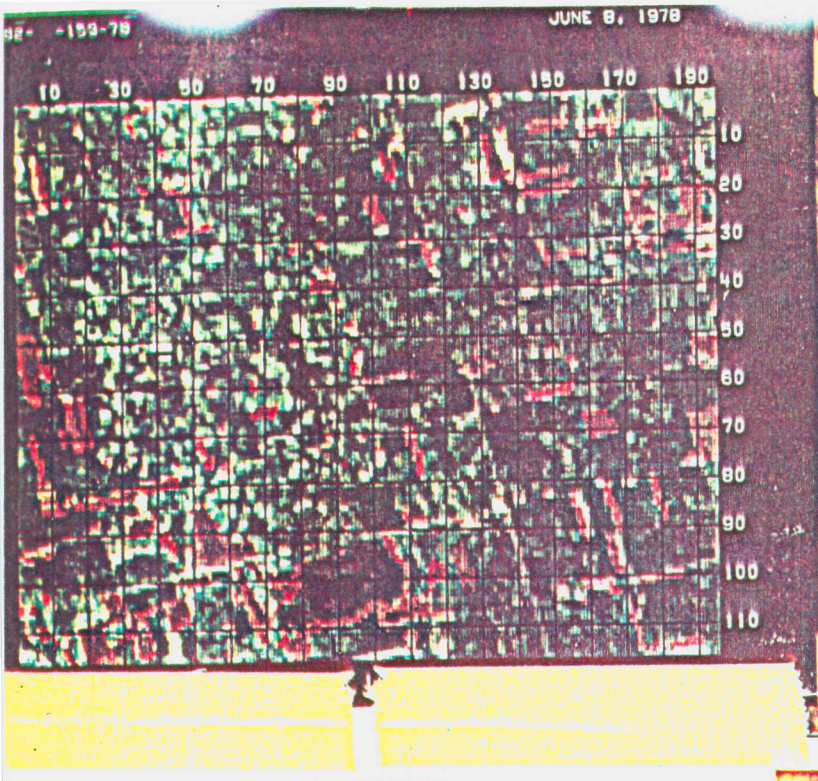
JUNE 8, 1978
10 30 50 70 90 110 130 150 170 190
10 20 30 40 50 60 70 80 90 100 110

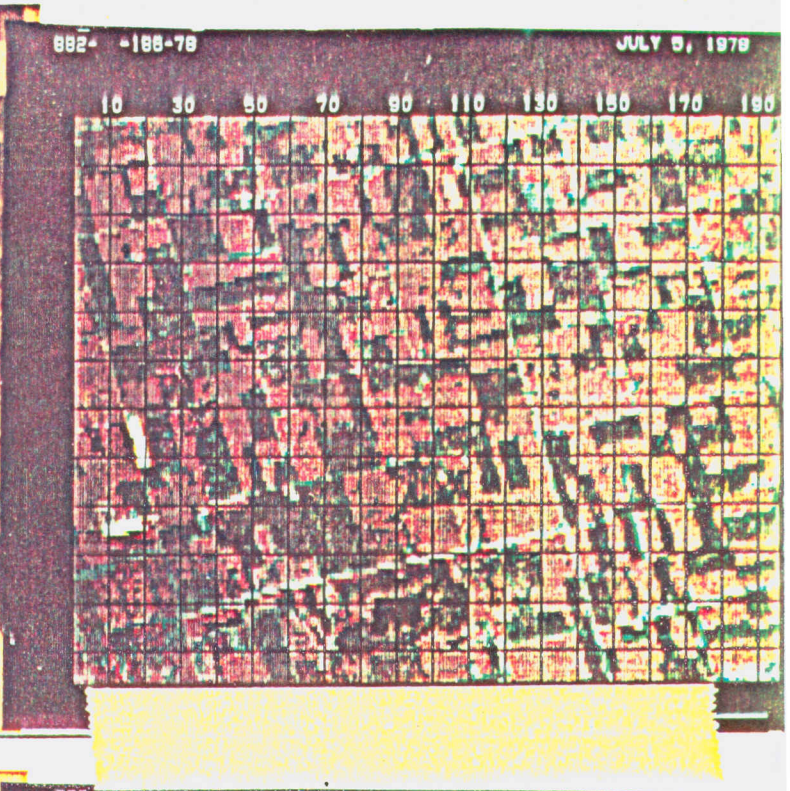
882- -188-78
JULY 9, 1978
10 30 50 70 90 110 130 150 170 190

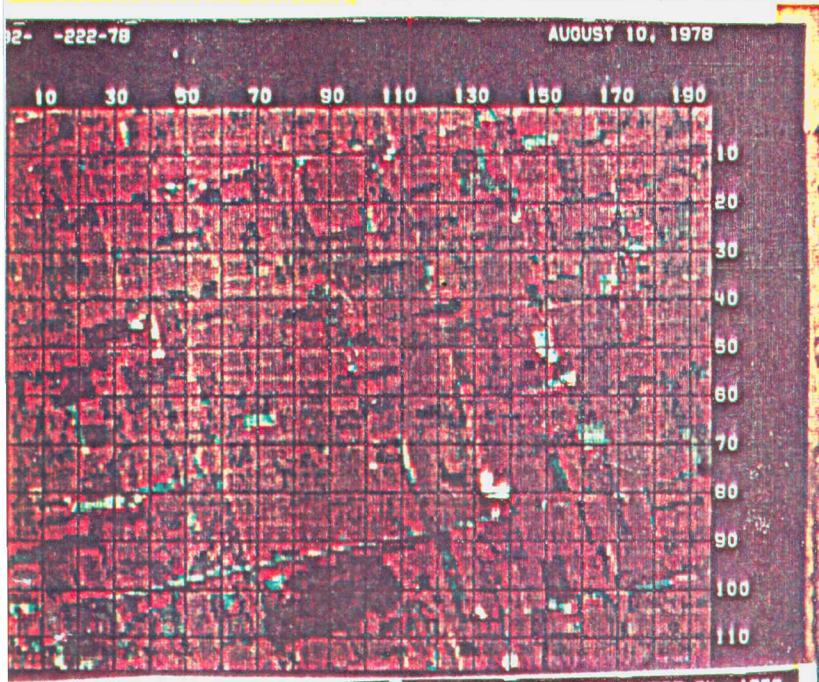
AUGUST 10, 1978
10 30 50 70 90 110 130 150 170 190
10 20 30 40 50 60 70 80 90 100 110

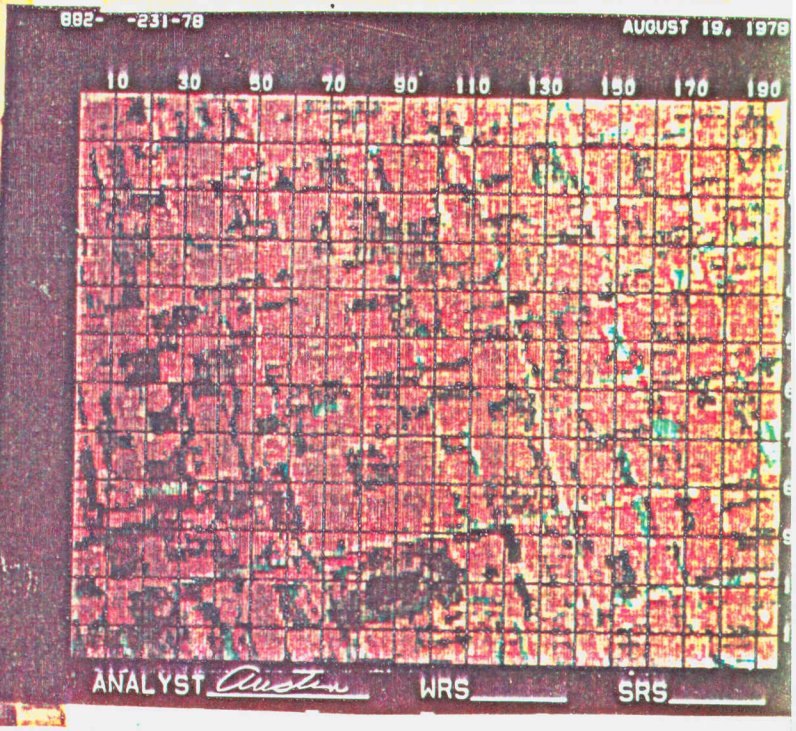
882- -231-78
AUGUST 19, 1978
10 30 50 70 90 110 130 150 170 190
ANALYST Austin WRS SRS


882- -267-78
SEPTEMBER 24, 1978
10 30 50 70 90 110 130 150 170 190
10 20 30 40 50 60 70 80 90 100 110

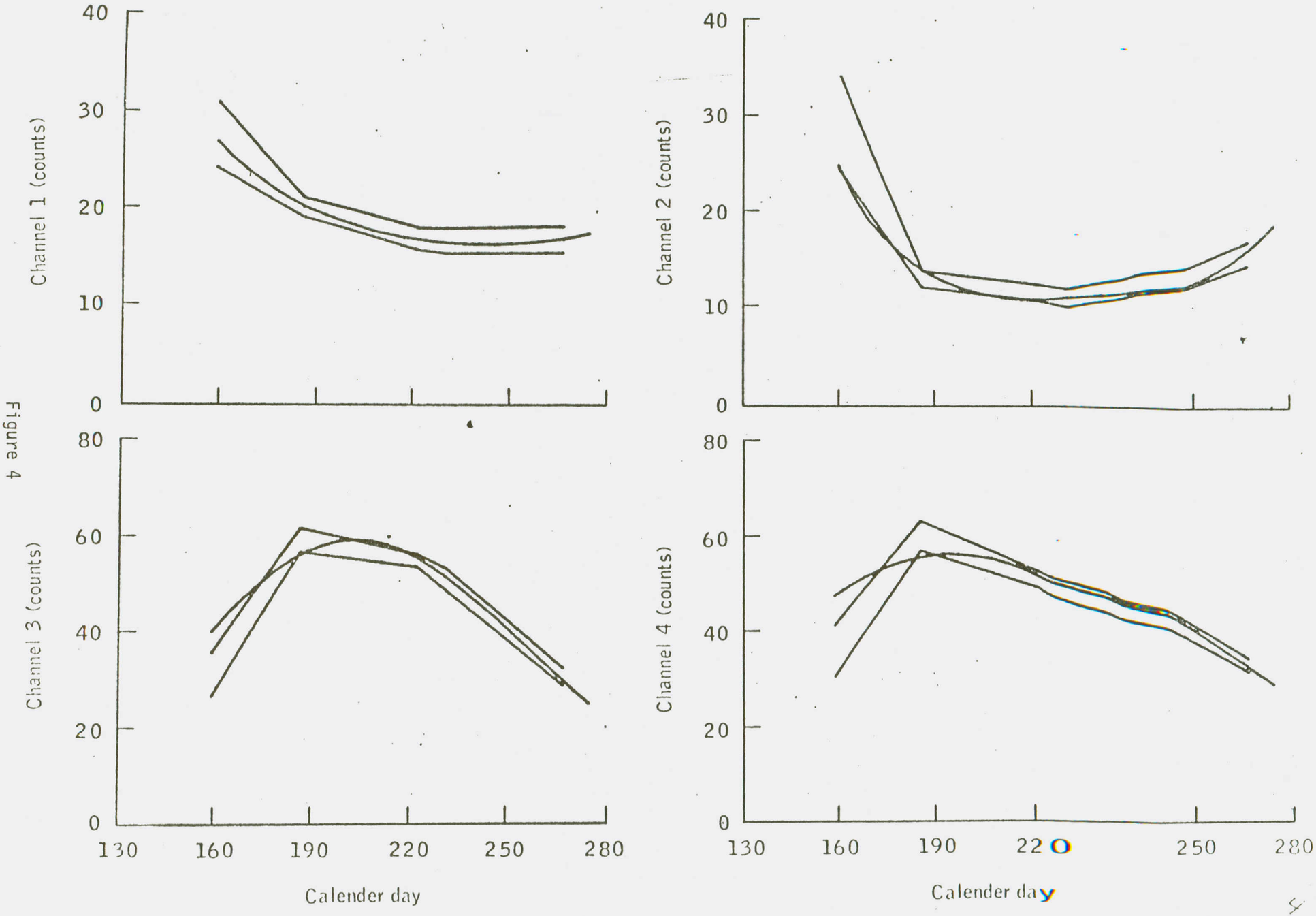
Channel 1 (counts)
40
30
20
10
0
Channel 2 (counts)
40
30
20
10
0
Channel 3 (counts)
80
60
40
20
0
Channel 4 (counts)
80
60
40
20
0
130
160
190
220
250
280
Calender day
Calender day

Figure 4

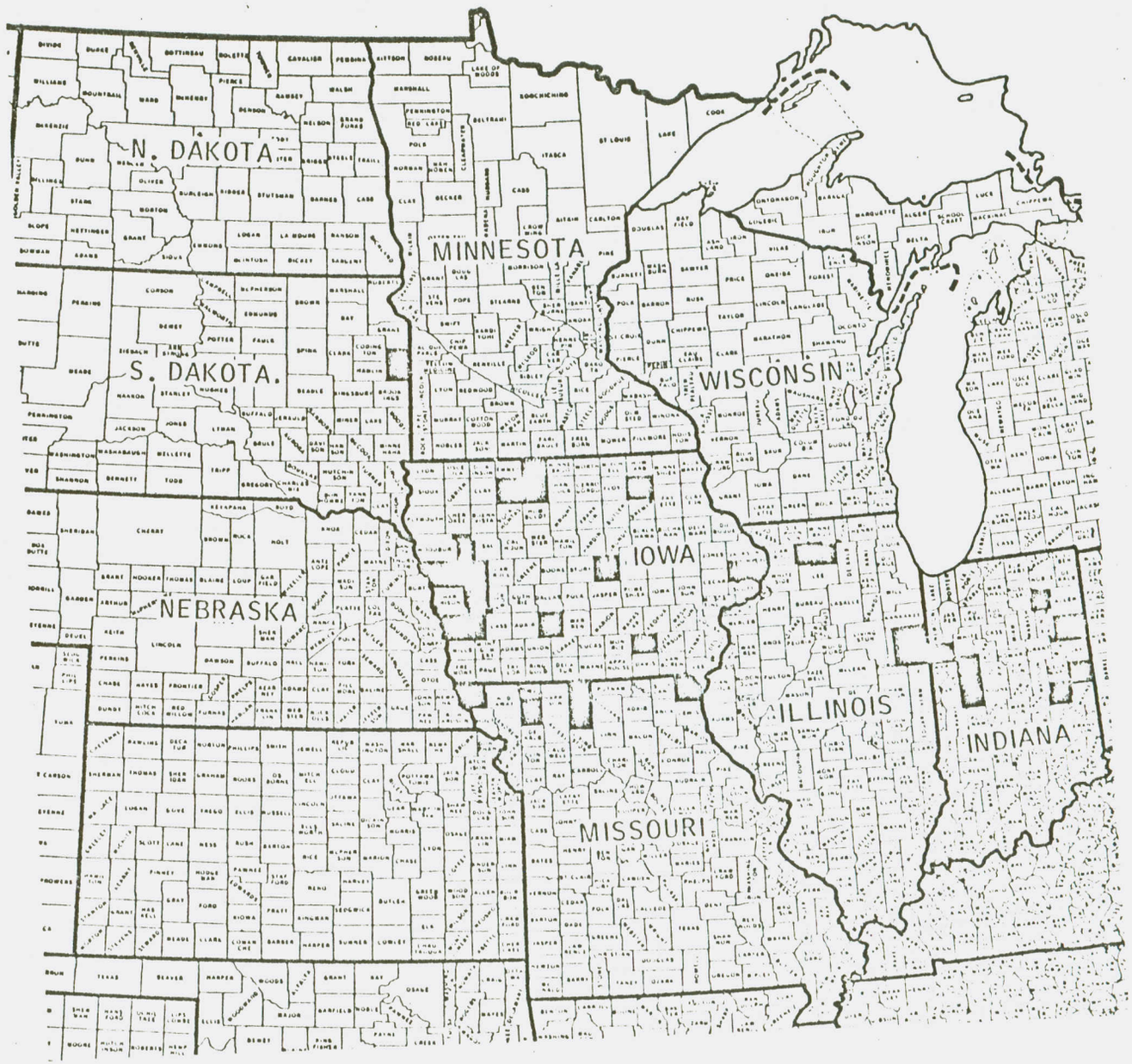
N. DAKOTA
MINNESOTA
S. DAKOTA.
WISCONSIN
IOWA
NEBRASKA
ILLINOIS
INDIANA
MISSOURI

Figure 5

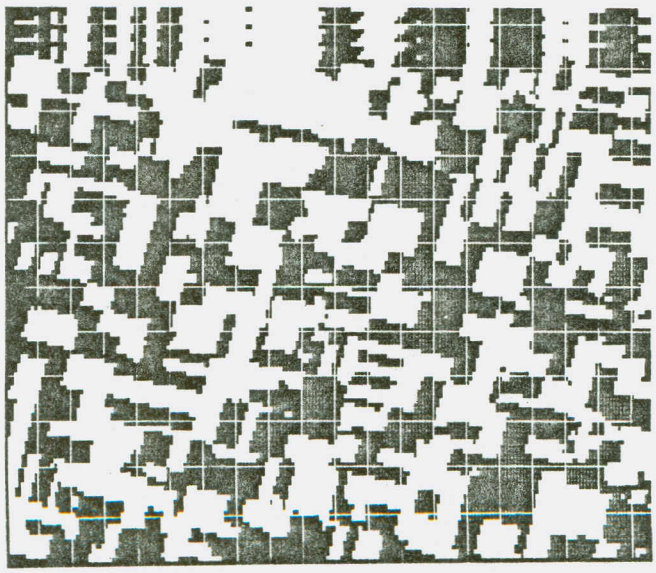

Figure 6

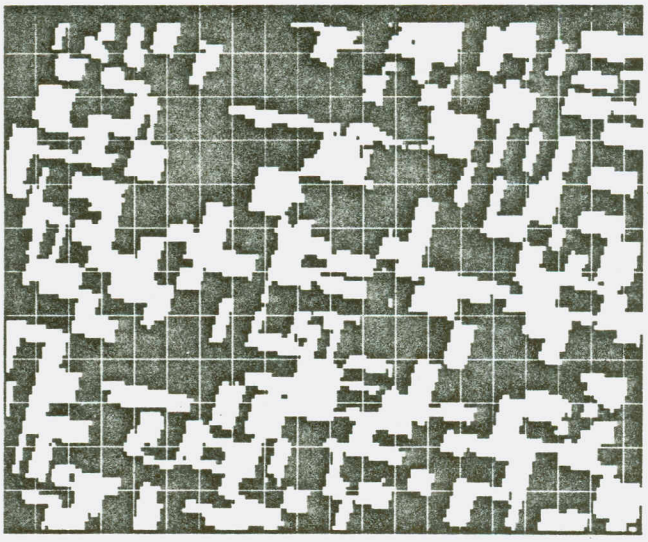

Figure 7

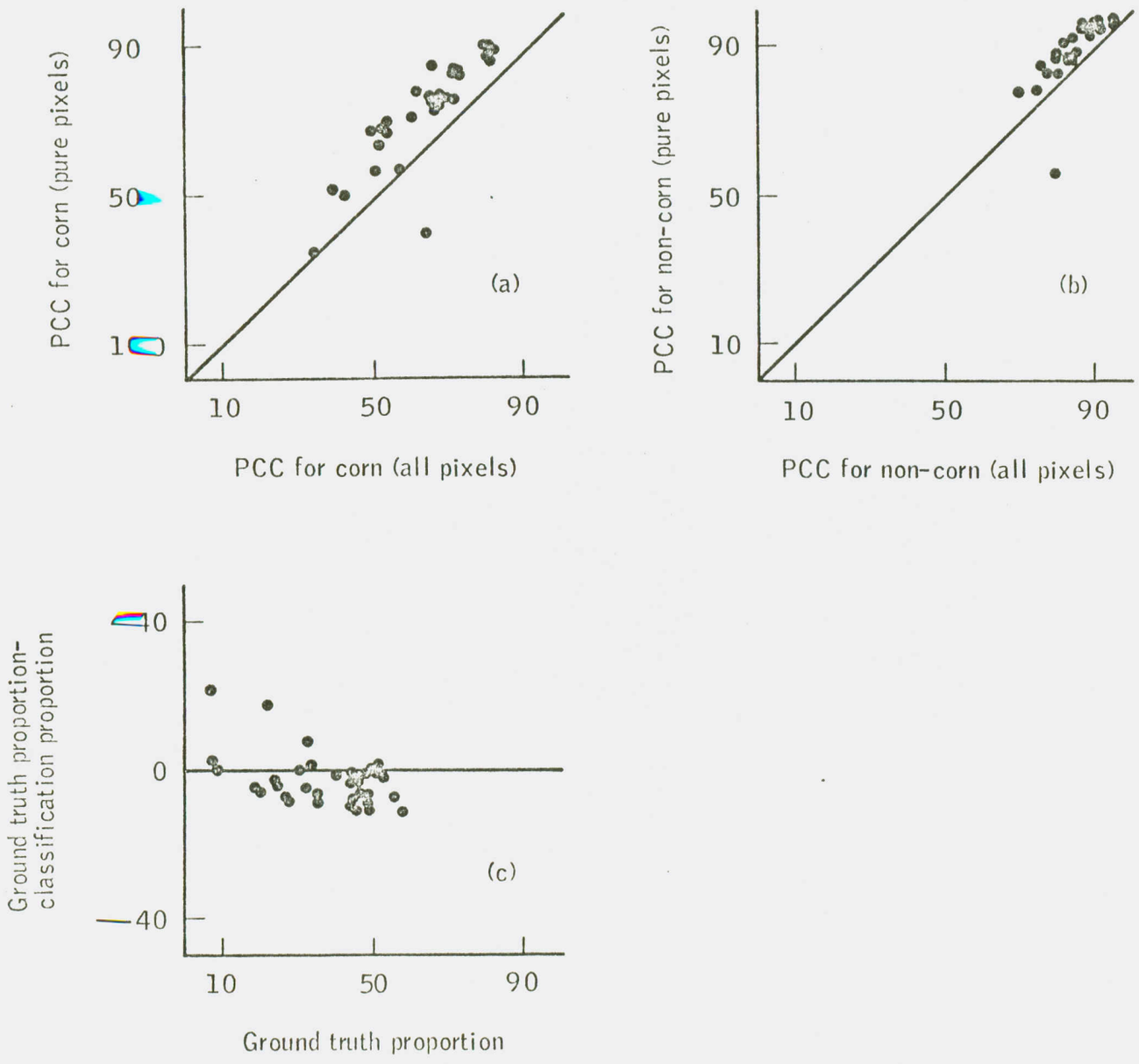
PCC for corn (pure pixels)
90
50
10
10
50
90
PCC for corn (all pixels)
(a)
PCC for non-corn (pure pixels)
90
50
10
10
50
90
PCC for non-corn (all pixels)
(b)
Ground truth proportion-classification proportion
40
0
-40
10
50
90
Ground truth proportion
(c)

Figure 8

Segment Number & Location	Acquisition Set (Julian Day) Training Field Coordinates (Line, Pixel)	Confusion Matrix C→C N→C	C→N N→N	Add scene % not ground truth identifier + pixels rejected as impure.
		(1) Superpure, (2) Pure, (3) All Pixel		
127	78161, 78216	28.2	3.9	
Montgomery, Indiana	78243, 78252	1.7	19.3	46.8
	(104,167), (101, 174)	35.3	5.9	
	(107,176), (110, 168)	5.5	34.5	17.9
		39.8	9.8	
		8.4	39.7	2.3
133	78152, 78197	8.8	4.4	
Whitley, Indiana	78233, 78251	2.0	16.4	68.4
	78269			
	(3,108), (3,115)	13.1	9.3	
	(8,117), (8,110)	2.5	39.7	23.4
		16.5	14.5	
		9.8	55.6	3.6
135	78166, 78229	14.1	5.2	
Chickasaw, Iowa	78247, 78265	1.6	16.7	62.4
	(25,146) (25,155)	20.7	8.6	
	(33,156) (33,147)	2.9	39.7	23.5
		25.3	12.9	
		11.1	47.0	3.8
141	78167, 78212	8.7	1.5	62.7
Madison, Iowa	78220, 78265	1.3	25.9	
	(46,148) (46,154)	13.0	4.6	
	(53,157) (53,152)	3.9	62.2	19.3
		15.7	8.4	
		5.6	69.5	4.7
144	78165, 78217	5.8	2.4	63.5
Wapello, Iowa	78246, 78264	0.5	27.7	
	(27,166) (27,172)	8.4	5.4	
	(40,178) (40,171)	2.6	64.2	19.3
		10.4	9.1	
		3.7	72.1	4.7
202	78167, 78212	4.1	7.5	
Atchison, Missouri	78221, 78266	4.4	30.4	53.6
	(3,119), (3,126)	6.4	11.7	19.1
	(9,130), (9,120)	9.3	53.5	
		8.0	15.5	
		11.2	59.7	5.7

Segment Number & Location	Acquisition Set (Julian Day) Training Field Coordinates (Line, Pixel)	Confusion Matrix (1) Superpure, (2) Pure, (3) All Pixels		Add scene % not ground truth identifie + pixels rejected as impure
		C→C	C→N	
		N→C	N→N	
205	78155, 78219	4.2	4.1	
	78246, 78272	1.9	38.4	51.5
Clark, Missouri	(48,169), (48,173)	5.9	7.1	
	(55,175), (56,172)	4.4	61.6	21.1
		7.2	9.9	
		5.6	68.0	9.3
209	78167, 78221	2.1	1.0	
	78247, 27266	1.4	41.5	53.9
Gentry, Missouri	78274	3.4	2.4	
	(11,187), (11,193)	3.7	74.4	16.1
	(13,193), (13,187)	4.0	4.2	
		4.2	80.1	7.5
211	78166, 78220	1.4	1.3	
	78247, 78265	1.8	35.1	60.4
Grundy, Missouri	78274	2.1	2.6	
	(50,122), (50,128)	5.6	71.6	18.2
	(55,128), (57,122)	2.6	4.1	
		6.5	77.5	9.3
216	78184, 78220	2.0	0.6	49.1
	78247, 27274	10.3	37.9	
Mercer, Missouri	(82,63), (80,74)	3.5	1.3	
	(85,75), (86,65)	19.8	61.0	14.4
		4.6	2.0	
		21.8	64.1	7.6
241	78187, 78205	7.9	4.5	
	78224, 78233	1.6	26.3	59.8
Devil, South Dakota	78251	11.2	8.1	
	(6,174), (6,185)	4.3	58.0	18.4
	(10,185), (10,177)	13.1	12.5	
		5.7	64.0	4.7
800	78164, 78219	24.6	8.3	
	78246, 78261	3.0	14.9	49.2
Clinton, Iowa	(68,14), (68, 34)	31.9	13.1	
	(70, 34), (70, 15)	6.5	27.5	21.0
		36.5	17.5	
		9.7	33.7	2.7

Segment Number & Location	Acquisition Set (Julian Day) Training Field Coordinates (Line, Pixel)	Confusion Matrix C→C N→C	Confusion Matrix C→N N→N	Add scene % not ground truth identified + pixels rejected as impure.
		(1) Superpure, (2) Pure, (3) All Pixels		
804 Marshall, Iowa	78166, 78229 78247, 78265	24.1 1.6	2.4 20.4	51.8
	(24,132), (23,141) (30,143), (31,133)	32.0 5.5	5.4 35.5	21.8
		36.6 8.1	9.5 42.0	3.8
809 Ogle, Illinois	78164, 78218 78244, 78271	23.9 1.8	7.4 11.8	55.2
	(43,6) (40,17) (47,20), (50,6)	31.6 4.6	12.8 25.8	25.1
		35.8 6.6	17.6 32.6	7.3
824 Iroquois, Illinois	78163, 78217 78235, 78243 78262	28.4 4.0	3.3 24.2	40.2
	(5,107), (5,118) (10,118), (10,107)	36.2 7.2	6.1 32.6	18.0
		40.8 10.3	9.1 36.9	2.9
832 Adams, Indiana	78151, 78160 78232, 78268	5.7 6.2	1.7 22.4	64.1
	(91,143), (91,153) (94,153), (94,143)	11.2 18.7	3.7 48.3	18.2
		15.6 23.0	5.9 53.1	2.4
837 Benton, Indiana	78180, 78198 78216, 78252	21.6 3.1	4.3 23.7	47.3
	(98,35), (96,47) (101,48), (104, 37)	27.7 8.1	8.1 38.1	18.1
		31.4 11.0	11.7 43.7	2.2
842 Henry, Indiana	78160, 78178 78232, 78250 78268	17.6 1.9	5.0 18.1	57.5
	(3,133), (3,145) (6,147), (9,137)	24.8 6.4	9.0 38.6	21.1
		29.1 9.9	13.7 44.9	2.4

Segment Number & Location	Acquisition Set (Julian Day) Training Field Coordinates (Line, Pixel)	Confusion Matrix (1) Superpure, (2) Pure, (3) All Pixels		Add scene % not ground truth identified + pixels rejected as impure.
		C→C N→C	C→N N→N	
843 Henry, Indiana	78178, 78197 78233, 78251 (13,121), (13,123) (22,127), (22,125)	12.2 3.3 19.1 12.2 23.6 16.1	2.5 18.8 5.2 44.7 8.6 50.4	63.2 18.7 1.3
852 Randolph, Indiana	78178, 78232 78250, 78268 (49,36), (49,44) (51,46), (53,37)	8.1 1.1 12.1 3.8 14.1 5.2	3.8 23.0 8.3 58.4 13.1 65.9	64.0 17.4 1.8
853 Randolph, Indiana	78160, 78178 78232, 78250 78268 (35,68), (34,72) (41, 77), (43,71)	9.1 0.7 14.0 5.6 17.4 8.4	6.9 19.1 12.4 47.8 17.3 55.3	64.2 20.2 1.6
854 Tippicanoe, Indiana	78161, 78207 78234, 78251 (73, 148), (73,155) (80,155), (80,148)	27.4 2.2 35.1 6.4 40.0 9.5	4.3 24.3 6.7 36.3 9.2 40.9	41.8 15.4 0.3
860 Wells, Indiana	78160, 78197 78232, 78251 78268 (91,61), (91,66) (95,67), (95,62)	9.6 2.1 14.3 6.9 18.3 9.9	2.8 25.0 6.3 47.3 10.0 54.5	60.4 25.2 7.3
864 Crawford, Iowa	78159, 78186 78231, 78267 (65,116), (65,120) (69,120), (69,116)	19.8 0.8 27.4 4.0 32.0 6.9	4.0 15.5 8.2 38.3 13.1 45.9	59.9 22.1 2.1

Segment Number & Location	Acquisition Set (Julian Day) Training Field Coordinates (Line, Pixel)	Confusion Matrix (1) Superpure, (2) Pure, (3) All Pixels		Add scen % not ground truth identifie + pixels rejected as impure
		C→C	C→N	
		N→C	N→N	
865	78168, 78186	11.4	3.1	
	78231, 78267	0.7	19.0	65.7
Crawford, Iowa	(7,71), (7,79)	16.5	7.4	
	(11,79), (11,71)	3.9	47.7	24.4
		20.3	12.8	
		6.3	56.0	4.7
877	78186, 78222	5.8	8.7	
	78231, 78267	8.6	11.0	65.7
Ida, Iowa	(70,114), (69, 123)	19.4	8.5	
	(75,125), (77, 117)	5.3	23.4	43.3
		24.5	13.7	
		8.3	32.2	21.4
878	78186, 78221	14.2	10.5	
	78266, 78293	1.9	26.0	47.4
Kossuth, Iowa	(9,140), (9,148)	20.5	15.0	
	(19,151), (19,144)	5.9	41.8	16.9
		24.4	18.7	
		8.7	47.3	0.9
880	78186, 78222	21.0	6.8	46.6
	78231, 78267	0.8	24.8	
Monona, Iowa	(46, 123), (46, 133)	26.5	11.2	
	(54, 136), (54, 127)	2.7	42.7	17.0
		29.1	15.7	
		4.7	48.8	1.6
881	78159, 78186	21.1	4.0	
	78222, 78231	0.5	20.6	53.8
Monona, Iowa	78267	27.5	7.6	
	(13, 81), (12, 90)	2.5	43.2	19.2
	(16, 90), (17, 82)	31.2	12.5	
		4.8	49.9	1.7
882	78159, 78186	23.6	2.4	
	78222, 78231	0.8	25.6	47.6
Palo Alto, Iowa	78267	30.4	5.0	
	(77,77),(76, 84)	2.9	40.0	21.7
	(81,87),(82, 80)	34.7	8.3	
		5.0	45.9	6.1

Segment Number & Location	Acquisition Set (Julian Day) Training Field Coordinates (Line, Pixel)	Confusion Matrix C→C N→C	C→N N→N	Add scene % not ground truth identified + pixels rejected as impure
		(1) Superpure, (2) Pure, (3) All Pixels		
883	78186, 78204	13.3	2.3	
	78213, 78221	3.4	25.7	55.4
Palo Alto, Iowa	78267	17.9	5.0	
		7.0	42.4	27.7
	(22,109) (22,118)			
	(29,120) (29,111)	21.2	8.5	
		9.6	49.0	11.6
886	78167, 78204	21.3	6.3	52.6
	78231, 78249	0.8	19.0	
Pottawatomi, Iowa	(102,77), (102,86)	27.2	11.0	
	(110,91), 110,81)	3.0	37.0	21.7
		30.4	16.6	
		5.4	43.7	4.0
891	78168, 78186	16.1	6.4	
	78204, 78267	2.0	10.0	65.5
Shelby, Iowa				
	(90,5), (90,13)	22.8	12.5	
	(97,13), (97,5)	6.4	31.3	27.1
		27.8	18.8	
		9.7	39.9	3.9
892	78167, 78204	24.7	2.4	
	78221, 78266	1.1	11.3	60.5
Shelby, Iowa				
	(16,50) (15,59)	34.1	5.6	
	(19,60) (19,53)	4.5	29.9	25.9
		40.1	10.4	
		8.1	36.9	4.5

References

1. K.S. Fu, D.A. Landgrebe and T. L. Phillips, Proc. IEEE, Vol. 57, 639 (1969).

2. R.S. Chikkara and D. Register, Technometrics, 21(4), 531 (1979).

3. R. M. Haralick, C.A. Hlanka, R. Yokoyama and S.M. Carlyle, IEEE Transactions on Geoscience & Remote Sensing, GE18, 167 (1980).

4. G.D. Badhwar, Photo. Eng. & Remote Sensing, 46, 369 (1980).

5. E.P. Crist and W. A. Malila, 11th Symposium on Remote Sensing of Environment, Costa Rica (1980).

6. R.J. Kauth, G. S. Thomas, LARS Symp. Proc. Machine Processing of Remotely Sensed Data (1976).

7. D. P. Rice, E.P. Crist and W. A. Malila, ERIM report 124000 (1980).

8. G.D. Badhwar and K.E. Henderson -"Development Stage Estimation of Corn from Spectral Data - An Initial Model" submitted to Ag. J. (1980).

9. D. Steiner and Salerno, A.E., Manual of Remote Sensing Chapter 12, 769 (1975).

10. Marquardt, D.W., J. Soc. Ind. Math. Vol. II (2), 431 (1963).

11. ERTS Data Handbook, Goddard Space Flight Center, (1975).

12. Duggin, M.J., 9th Symposium on Remote Sensing of Environment, Michigan (1974).

13. D.E. Pitts et al, J. Appl, Meteor. 16, (12), 1977.

14. W.J. Conover, Practical Nonparametric Statistics, John Wiley & Sons, Inc. 295-303, (1971).

"A Semi-Automatic Technique for Multitemporal Classification of a Given Crop of a Lansat Scene"

SUPPORTING RESEARCH
TECHNICAL REPORT

SR-JO-04001
JSC-16829

January 12, 1981

DISTRIBUTION

- Distribution of this document is limited to those people whose names appear without an asterisk. Persons with an asterisk(*) beside their name will receive an abstract only (JSC Form 1424).
- To obtain a copy of this document, contact one of the following:

  F. G. Hall - (SG3)
  J. E. Wainwright - Lockheed Development & Evaluation Department (626-43) (C09)

SK/R. Erb*
J. Powers *
R. Hatch (USDA) *
W. Stephenson *
M. Helfert *
F. Barrett (USDA) *
L. Childs
G. Nixon *

SG/R. MacDonald

SG2/D. Hay
R. Musgrove
W. Weimer *
D. Frank (USDA) *
G. McKain *

SG3/F. Hall
M. Ferguson
C. Hallum
R. Heydorn
A. Houston
D. Thompson
D. Pitts
A. Feiveson
R. Juday
M. Steib
K. Henderson
J. Dietrich

Oregon State University
L. Eisgruber

GMI/R. Holmes

Data Resources, Inc.
B. Scherr

Kansas State University/
E. T. Lab
E. Kanemasu

SH2/R. Hill
D. Amsbury *
K. Demel *
K. Hancock *
N. Hatcher *
R. Joosten *
T. Pendleton
C. Forbes *
L. Bennett *
M. Trichel

SH3/J. Dragg
R. Eason *
R. Bizzell
D. Henninger
W. Jones *
G. Kraus *
R. McKinney *
H. Prior *
F. Ravet *
L. Wade *
V. Whitehead *
K. Baker *
J. Carney *
C. Davis
G. Gutschewski *
F. Herbert *
F. Johnson *
R. Patterson *
J. Ginns *

Tom Barnett/NOAA CEAS *
116 Federal Building
Columiba, MO 65201

LOCKHEED
C09/J. G. Baron *
M. L. Bertrand *
B. L. Carroll
P. L. Krumm *
T. C. Minter
D. E. Phinney
P. C. Swanzy *
J. J. Vaccaro *
J. E. Wainwright (3)
J. L. Hawkins (2)
** Job Order File

** B09/Technical Library (5)

ERIM/R. Horvath (4)

PURDUE-LARS/M. E. Bauer (4)

PURDUE University
Dr. Paarlberg

TAMU/L. F. Guseman

UCB/C. M. Hay

IBM- Houston, TX MC16/
A. Anderson

IBM - Palo Alto, CA/Dr. Kolsky

USDA - Houston, TX
G. Boatwright

USDC - Washington, D.C./
R. Ambroziak

USDC/EDIS/CEAS - Columbia, MO
S. LeDuc
C. Sakamoto

** LOCKHEED Documents Only